Journal of Geophysical Research: Oceans

Supporting Information for

Mississippi river chemistry impacts on the interannual variability of aragonite saturation state in the Northern Gulf of Mexico

Fabian A. Gomez[1,2], Rik Wanninkhof[2], Leticia Barbero[3,2], Sang-Ki Lee[2]

[1]Northern Gulf Institute, Mississippi State University, Starkville, Mississippi, USA.

[2]NOAA Atlantic Oceanographic and Meteorological Laboratory, Miami, Florida, USA.

[3]Cooperative Institute for Marine and Atmospheric Studies, University of Miami, Miami, Florida, USA.

Contents of this file

Introduction

Additional information supporting our study is provided below. Figure S1 presents relationships linking discharge and both alkalinity and dissolved inorganic carbon (DIC) anomalies in the Mississippi River. Figure S2 shows high-discharge composites for additional biogeochemical variables. Figure S3 displays climatological patterns for aragonite saturation state. Figures S4-S7 present composites for low-discharge conditions. Figures S8-S11 show supporting results for the model sensitivity analysis. Figure S12 contains similar histograms as in Figure 7 but for 1980-1999. Table S1 shows the selected periods for the composite analysis, and Table S2 details differences between the model hindcast and the sensitivity experiments. Tables S3-S4 contain supplementary statistics for the analysis in Section 3.3.

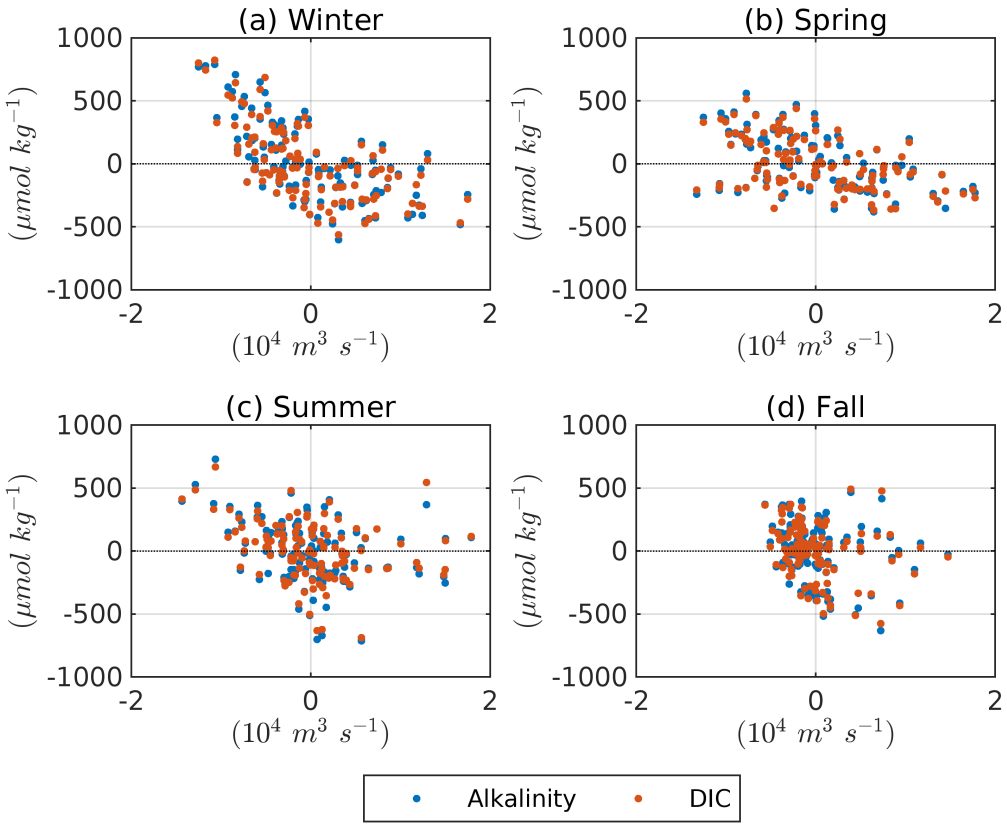

Figure S1. Mississippi River's anomalies of alkalinity and DIC against discharge anomalies. Patterns were derived from monthly averaged records during 1980-2019. Patterns were derived from the U.S. Geological Survey records.

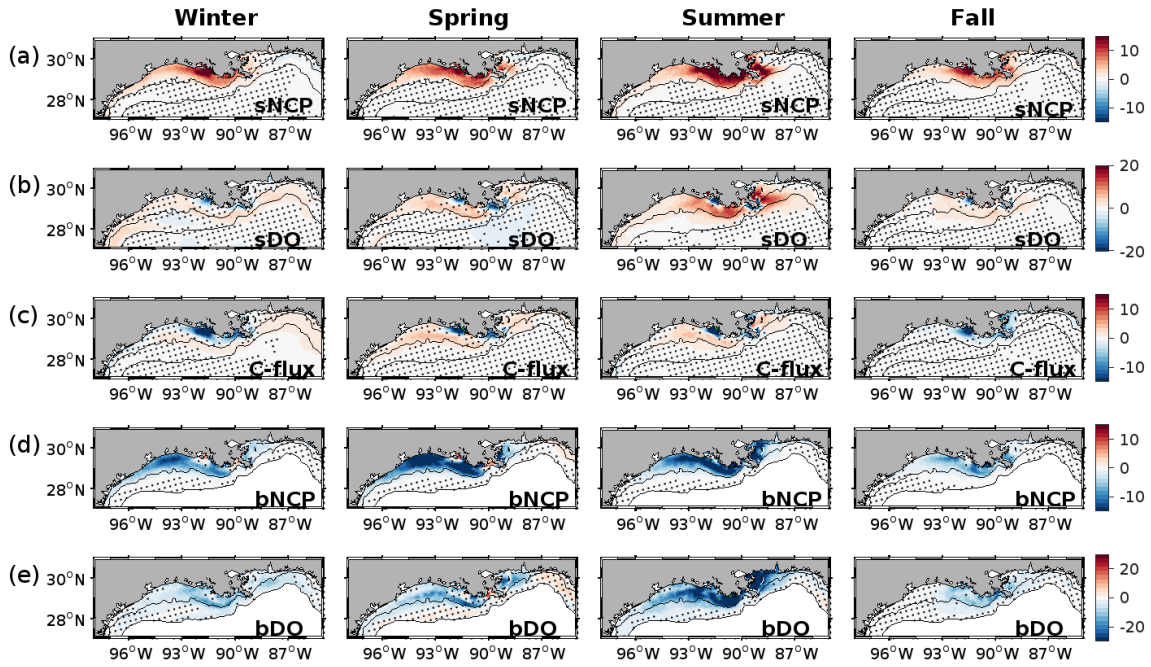

Figure S2. High discharge composites of the hindcast anomalies of (a) surface net community production (*s*NCP), (b) surface dissolved oxygen (*s*DO), (c) air-sea CO_2 flux (C-flux), (d) bottom net community production (*b*NCP), and (e) bottom dissolved oxygen (*b*DO) (e) during winter, spring, summer, and fall. Anomaly series were detrended before estimating the composites. Black contours depict the 25 m and 200 m isobaths. Anomalies are in mmol m^{-3} day^{-1} for NCP and C-flux, and µmol kg^{-1} for DO. Negative C-flux anomalies imply decreased carbon uptake or enhanced carbon outgassing. Dotted area represents non-significant values.

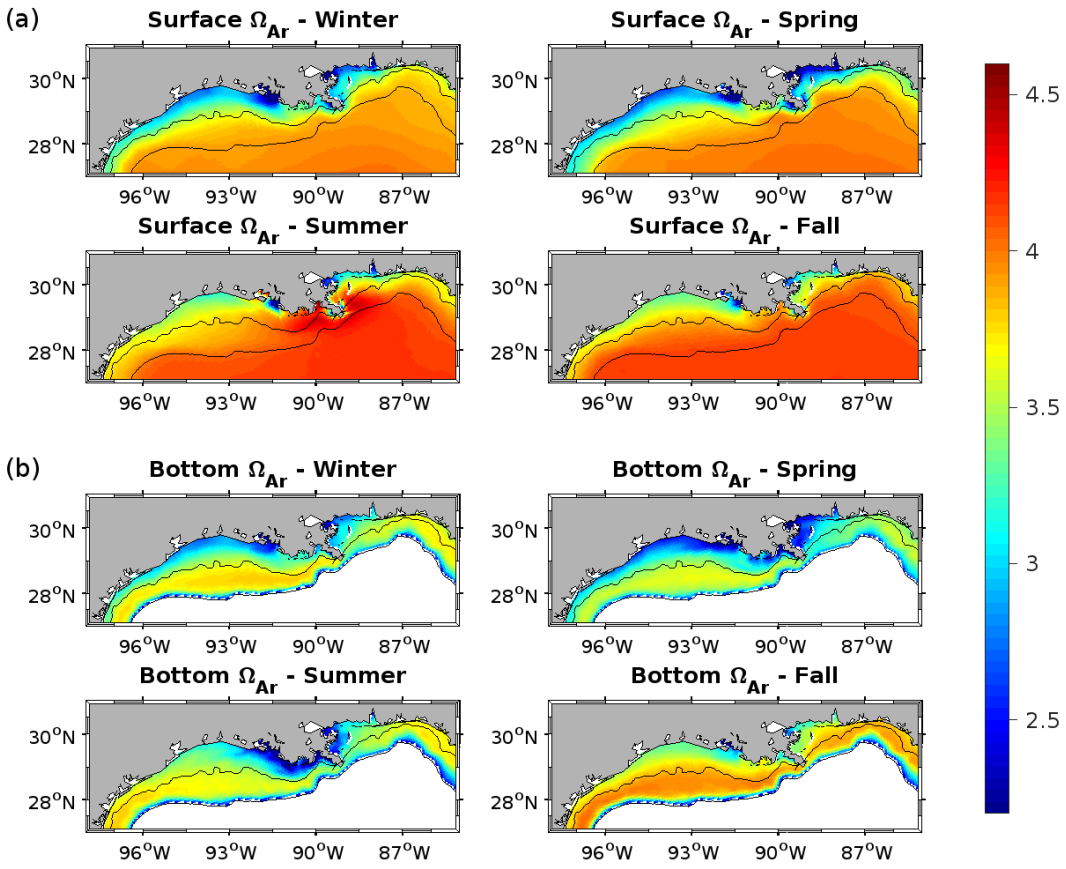

Figure S3. Seasonal climatology for (a) surface and (b) bottom aragonite saturation state (Ω_{Ar}) during 1980-2019 as derived from the model hindcast.

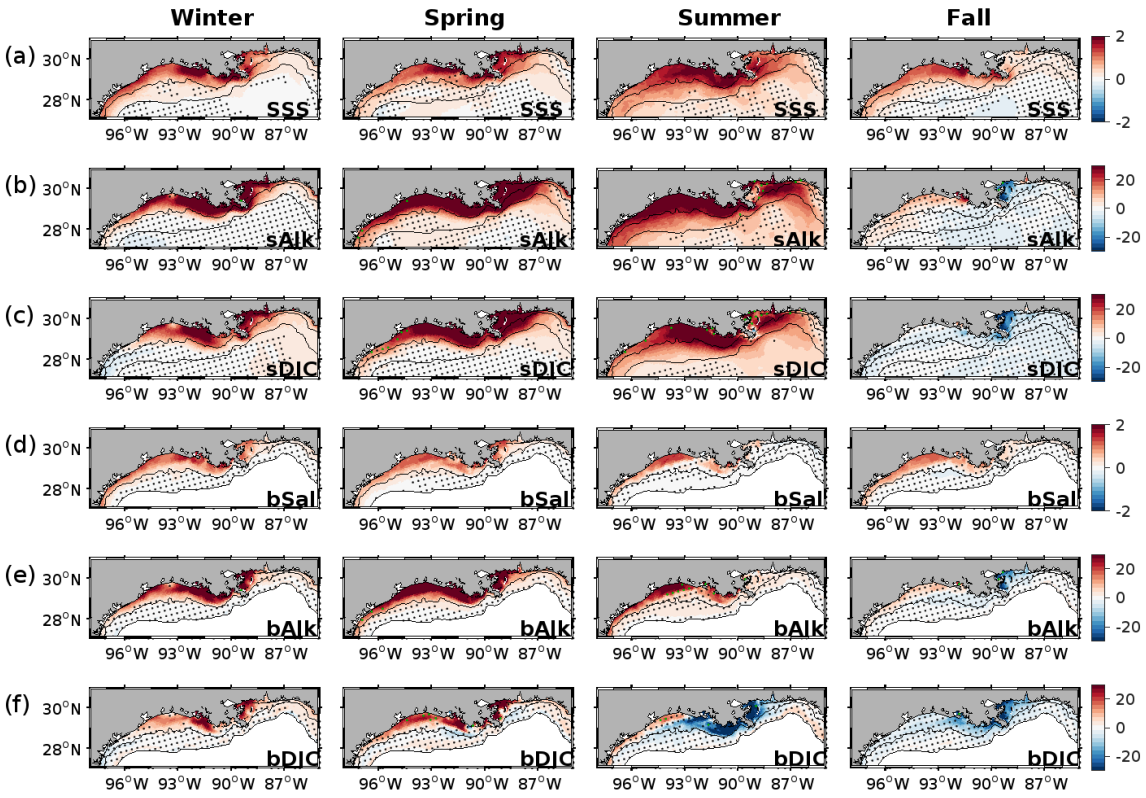

Figure S4. Low discharge composites of the hindcast anomalies of (a) sea surface salinity (SSS), (b) surface alkalinity (*s*Alk), (c) surface DIC (*s*DIC), (d) bottom salinity (*b*Sal), (e) bottom alkalinity *(b*Alk), and (f) bottom DIC (*b*DIC) during winter, spring, summer, and fall. Anomaly series were detrended before estimating the composites. Black contours depict the 25 m and 200 m isobaths. Alkalinity and DIC anomalies are in μmol kg^{-1}. Dotted area represents non-significant values.

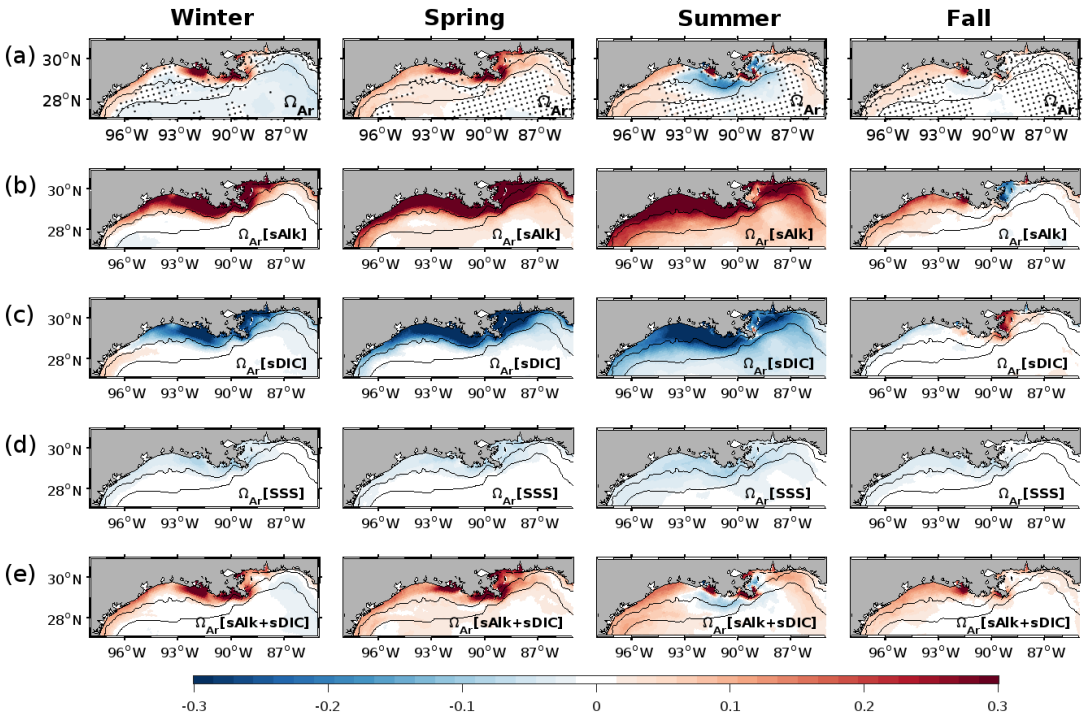

Figure S5. (a) Low discharge composites of surface aragonite saturation during winters, springs, summers, and falls, as derived from the model hindcast; (b–e) Taylor decomposition terms of the composite's patterns, representing changes induced by (b) surface alkalinity (sAlk), (c) surface DIC, (d) sea surface salinity (SSS), and (e) the added effect of sAlk and sDIC. The temperature term was omitted since it has a residual impact in the composite. Anomaly series were detrended before estimating the composites. Dotted area in (a) represents non-significant anomalies. Black contours depict the 25 m and 200 m isobaths.

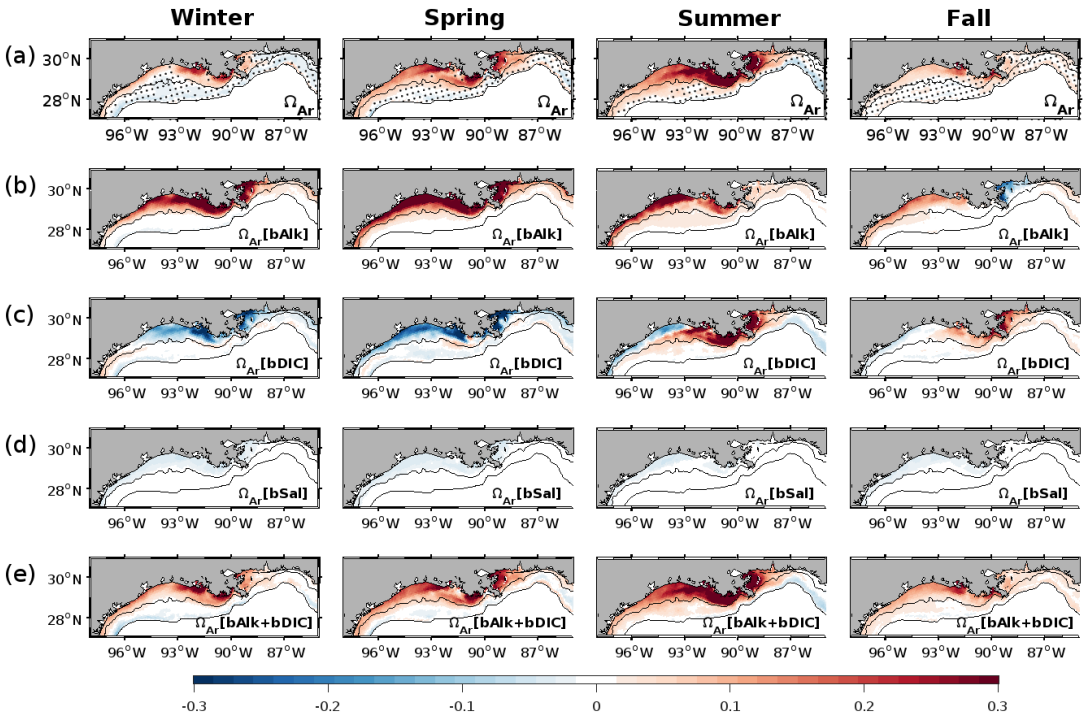

Figure S6. As Figure S5 but for bottom aragonite saturation.

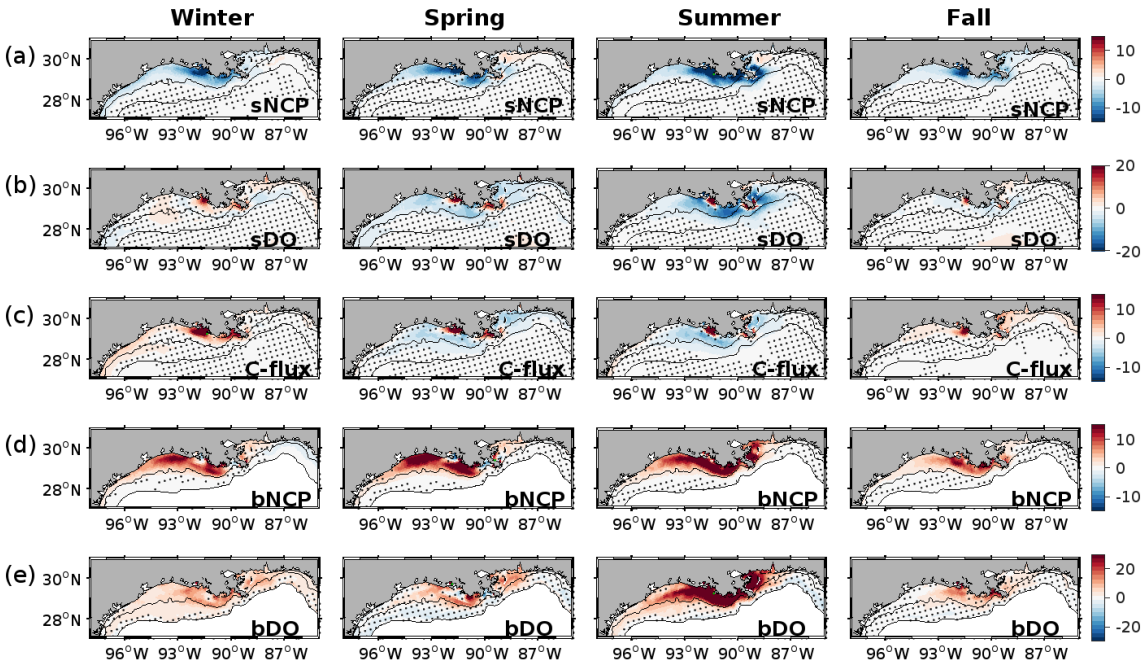

Figure S7. As Figure S2 but for low discharge conditions.

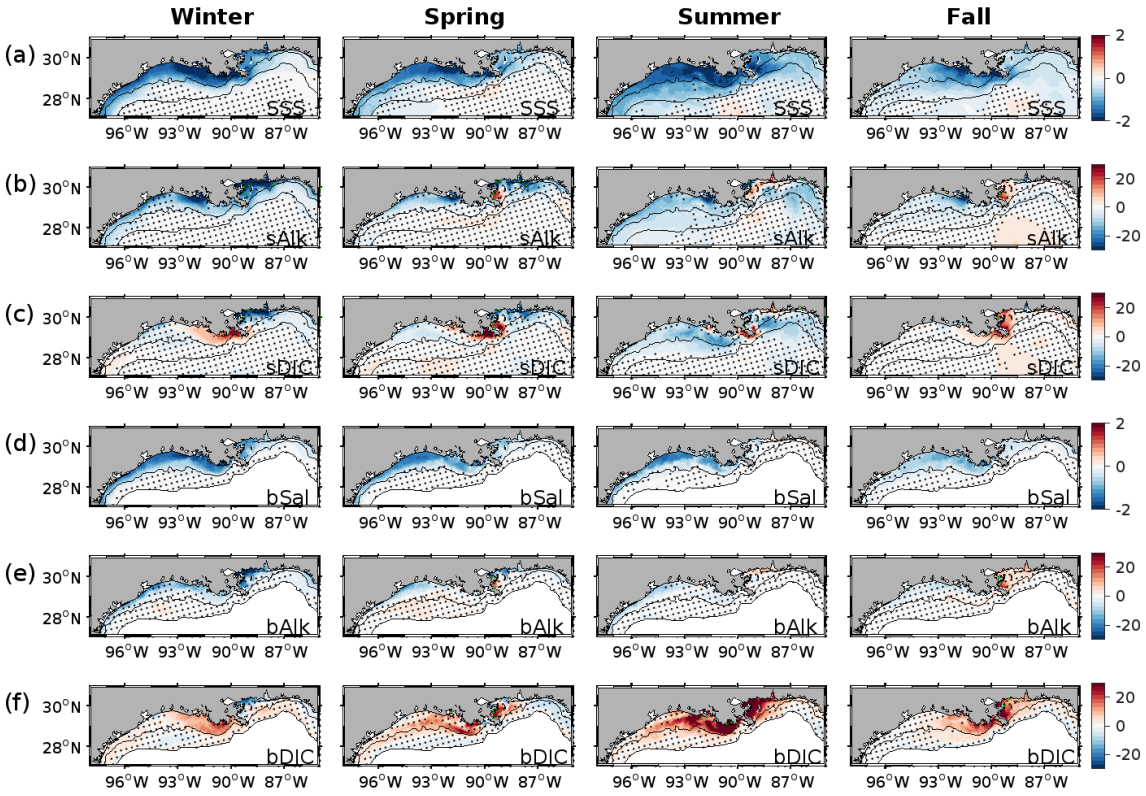

Figure S8. High discharge anomaly composites derived from the Constant Carbonate experiment: (a) sea surface salinity (SSS), (b) surface alkalinity (*s*Alk), (c) surface DIC (*s*DIC), (d) bottom salinity (*b*Sal), (e) bottom alkalinity (*b*Alk), and (f) bottom DIC (*b*DIC) during winter, spring, summer, and fall. Anomaly series were detrended before estimating the composites. Black contours depict the 25 m and 200 m isobaths. Alkalinity and DIC anomalies are in μmol kg^{-1}. Dotted area represents non-significant values.

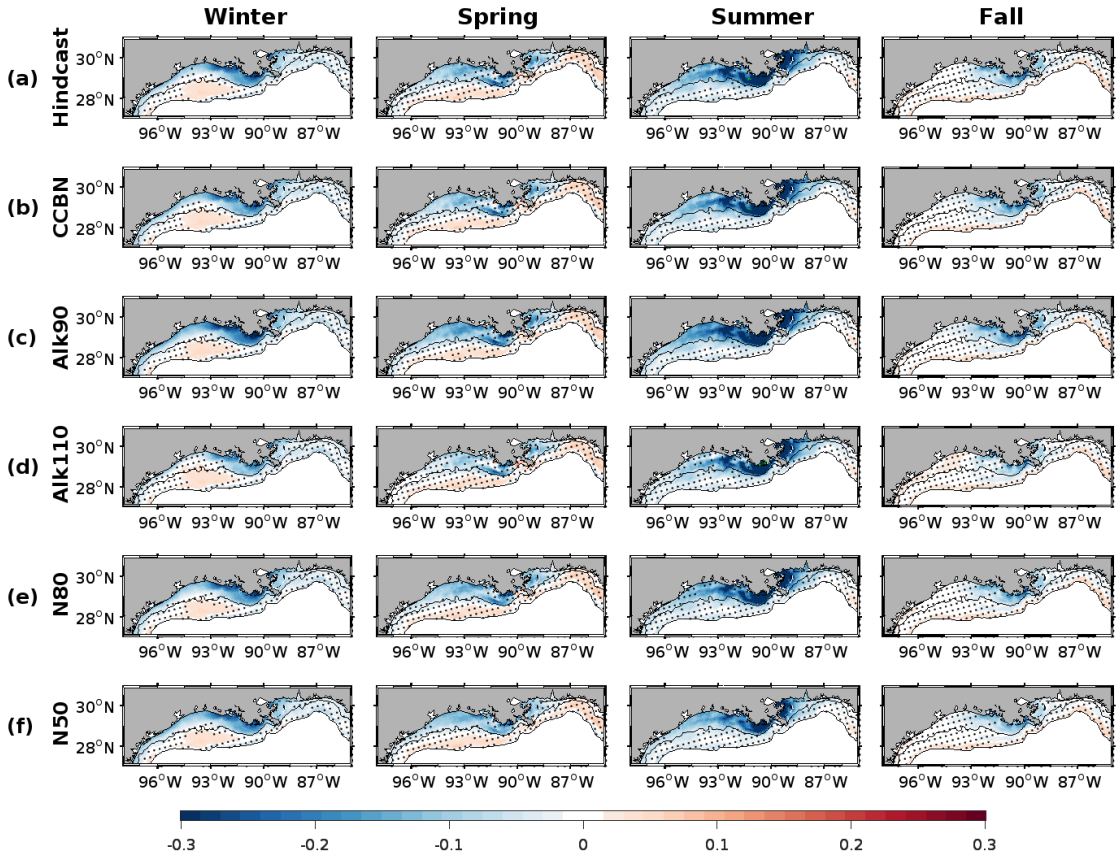

Figure S9. High discharge composites of the mean bottom Ω_{Ar} anomaly derived from the following experiments: (a) Hindcast, (b) Constant Carbonate (CCBN), (c) Alkalinity 90% (Alk90), (d) Alkalinity 110% (Alk110), (e) Nitrate 80% (N80), and (f) Nitrate 50% (N50). Anomaly series were detrended before estimating the composites. Black contours depict the 25 m and 200 m isobaths. Dotted area represents non-significant values.

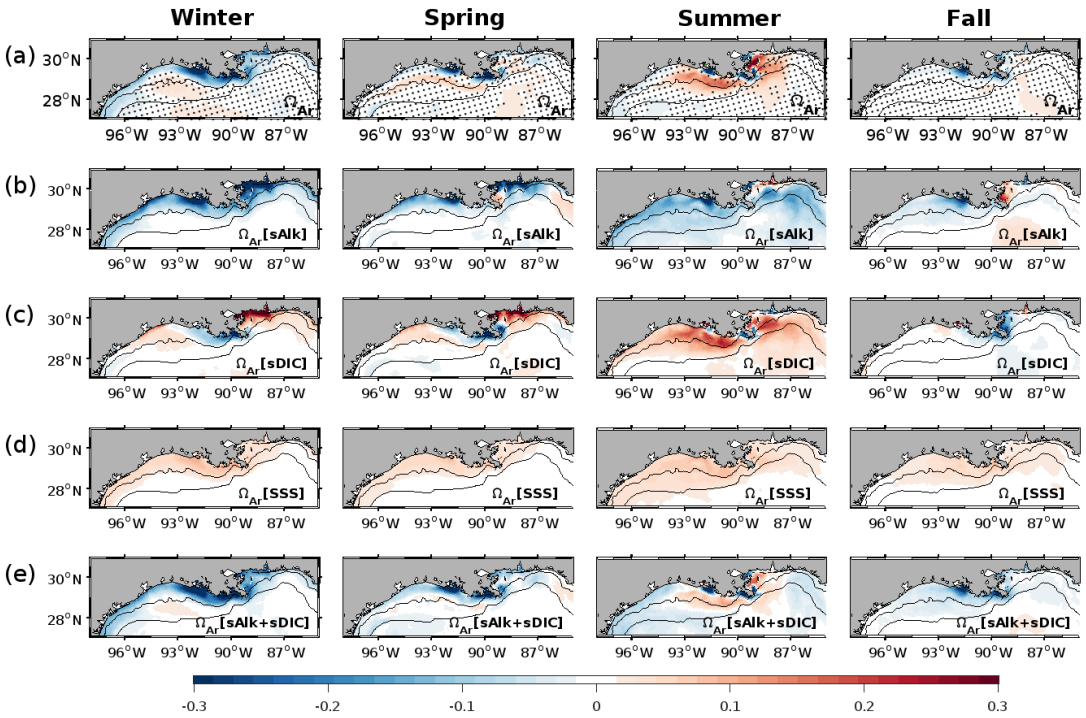

Figure S10. (a) High discharge composites of surface aragonite saturation derived from the Constant Carbonate experiment; (b–e) Taylor decomposition terms of the composite's patterns, representing changes induced by (b) surface alkalinity (sAlk), (c) surface DIC, (d) sea surface salinity (SSS), and (e) the added effect of sAlk and sDIC. Anomaly series were detrended before estimating the composites. Dotted area in (a) represents non-significant anomalies. Black contours depict the 25 m and 200 m isobaths.

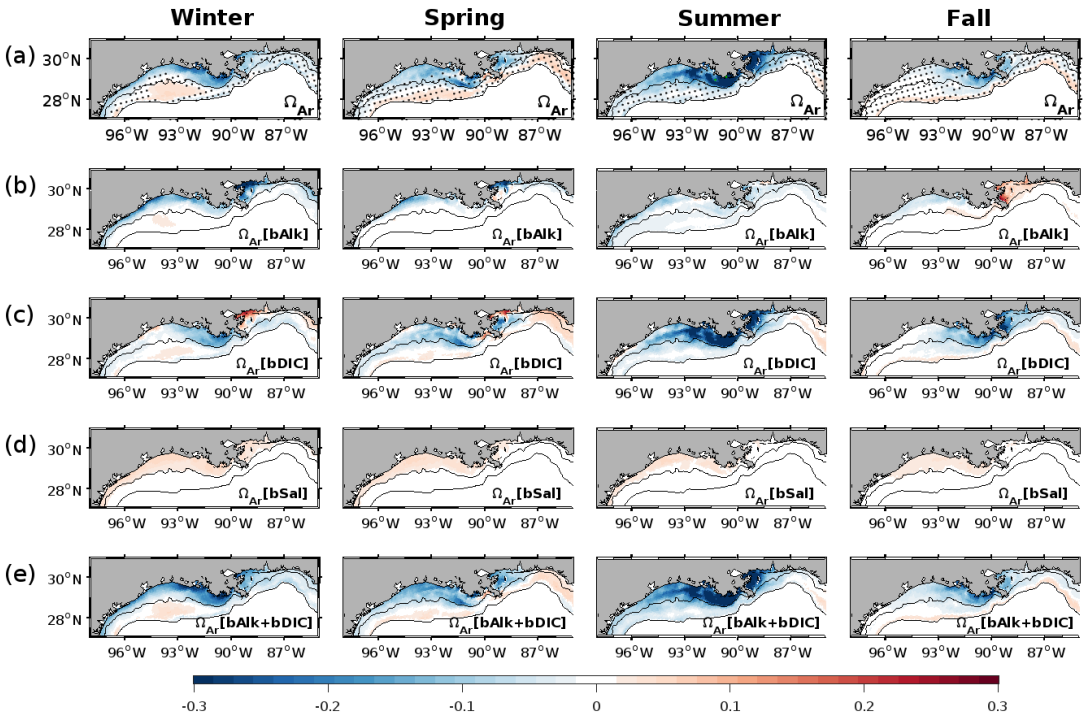

Figure S11. As Figure S10 but for the bottom Ω_{Ar} anomalies.

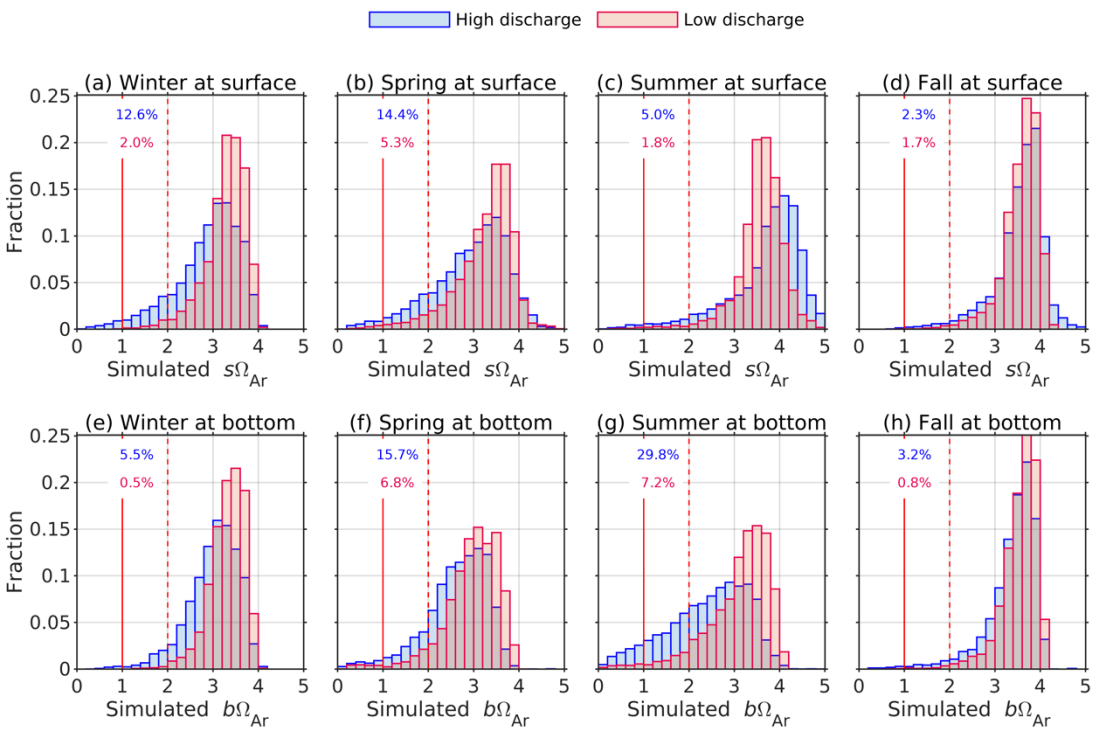

Figure S12. Frequency histograms for the simulated surface (a-d) and bottom (e-h) aragonite saturation state over the northern Gulf inner shelf (<25 m bottom depth; 93°–89°W) during the high and low discharge conditions from 1980-1999: (a, e) winter, (b, f) spring, (c, g) summer, and (d-h) fall. Blue and red numbers at each panel indicate the percentage of suboptimal values (Ω_{Ar} < 2) during high and low discharge, respectively.

Year	Winter (DJF)	Spring (MAM)	Summer (JJA)	Fall (SON)	Year	Winter (DJF)	Spring (MAM)	Summer (JJA)	Fall (SON)
1980			Low		2000	Low	Low	Low	Low
1981	Low	Low			2001	Low			
1982	Low				2002				
1983	High		High	Low	2003		Low		
1984			High		2004				
1985	High		Low		2005	High		Low	Low
1986	High	Low		High	2006	Low	Low	Low	Low
1987			Low	Low	2007			Low	
1988			Low	Low	2008		High	High	High
1989		High			2009				High
1990	Low	High	High		2010	High			High
1991	High	High		Low	2011	Low		High	
1992		Low	Low	High	2012			Low	Low
1993	High	High	High	High	2013	Low			
1994		High			2014		Low		
1995		Low	High		2015			High	High
1996	Low	Low			2016	High	High		High
1997	High	High		Low	2017		Low	High	
1998					2018	Low	High		High
1999				Low	2019	High	High	High	High

Table S1. Selected years for the high (light blue) and low (green) MARS discharge composites during winter, spring, summer, and fall. The selected high/low discharge years for winter (December-February), spring (March-May), summer (June-August), and fall (September-October).

Experiment	River chemistry	River water discharge
Hindcast	Time-evolving for the MARS; climatological for other rivers.	Time-evolving for the MARS and 26 main rivers in the USA; climatological mean for 10 rivers in the USA and 11 rivers in Mexico
CCBN	Long-term annual average for MARS's alkalinity and DIC; everything else as in the model hindcast	As in the model hindcast
Alk090	MARS alkalinity reduced by 10%; everything else as in the model hindcast	As in the model hindcast
Alk110	MARS alkalinity increased by 10%; everything else as in the model hindcast	As in the model hindcast
N80	MARS nitrate reduced by 20%; everything else as in the model hindcast	As in the model hindcast
N50	MARS nitrate reduced by 50%; everything else as in the model hindcast	As in the model hindcast

Table S2. Type of inputs used in the hindcast and five sensitivity experiments: Constant Carbonate (CCBN), Alkalinity 90% (Alk090), Alkalinity 110% (Alk110), Nitrate 80% (N80), and Nitrate 50% (N50).

	Season	Layer	MARS discharge condition	Median	Standard Deviation	[Ω_{Ar}<2] (%)	[Ω_{Ar}<1] (%)	Skewness
2000-2019	Winter	Surface	High	2.85	0.65	**14.6**	1.9	-0.95
			Low	3.19	0.47	3.3	0.1	-1.24
		Bottom	High	2.88	0.51	7.2	0.4	-0.87
			Low	3.18	0.41	1.7	0.1	-1.23
	Spring	Surface	High	3.17	0.78	**12.0**	2.2	-0.88
			Low	4.42	0.67	5.1	0.4	-0.86
		Bottom	High	2.66	0.67	**16.8**	2.6	-0.81
			Low	2.92	0.63	8.6	1.9	-1.19
	Summer	Surface	High	3.72	0.79	4.0	1.0	-0.78
			Low	3.77	0.59	1.0.	0.1	-0.38
		Bottom	High	2.46	0.82	**32.8**	**7.4**	-0.49
			Low	3.33	0.60	5.3	1.1	-1.67
	Fall	Surface	High	3.51	0.49	2.1	0.0	-1.44
			Low	3.65	0.35	0.1	0.0	-1.14
		Bottom	High	3.36	0.47	2.5	0.4	-1.79
			Low	3.58	0.35	0.5	0.2	-2.15
1980-1999	Winter	Surface	High	3.02	0.71	**12.6**	2.1	-1.00
			Low	3.35	0.44	2.0	0.0	-1.30
		Bottom	High	3.09	0.55	5.5	0.6	-0.97
			Low	3.37	0.38	0.5	0.0	-1.03
	Spring	Surface	High	3.08	0.82	**14.4**	0.8	-0.77
			Low	3.41	0.64	5.3	0.8	-1.27
		Bottom	High	2.74	0.69	**15.7**	3.2	-0.99
			Low	3.05	0.61	6.8	1.7	-1.36
	Summer	Surface	High	3.93	0.87	5.0	1.3	-1.09
			Low	3.63	0.53	1.8	0.4	-1.60
		Bottom	High	2.57	0.88	**29.8**	**8.3**	-0.52
			Low	3.27	0.69	7.2	1.9	-1.42
	Fall	Surface	High	3.67	0.56	2.3	0.2	-1.41
			Low	3.66	0.41	0.7	0.0	-1.62
		Bottom	High	3.51	0.56	3.2	0.7	-1.92
			Low	3.63	0.41	0.8	0.1	-1.81

Table S3. Statistics of the hindcast-derived frequency distributions of Ω_{Ar} over the inner-shelf between 93°–89°W during high and low discharge conditions. [Ω_{Ar}<2] and [Ω_{Ar}<1] represent the percentage of monthly Ω_{Ar} outputs below the threshold of 2 and 1, respectively. The [Ω_{Ar}<2] greater than 10%, and the [Ω_{Ar}<1] greater than 5%, are highlighted in blue and red color, respectively.

	Layer	MARS discharge condition	Hindcast	CCBN	Alk90	Alk110	N80	N50
Winter	Surface	High	14.6	14.5	22.1	6.7	14.8	15.0
		Low	3.3	3.9	7.4	0.8	3.4	3.5
	Bottom	High	7.2	6.9	12.4	3.6	7.2	7.2
		Low	1.7	1.9	2.9	0.9	1.7	1.6
Spring	Surface	High	12.0	11.1	19.7	5.5	12.3	13.1
		Low	5.1	5.0	8.4	2.3	5.3	5.6
	Bottom	High	16.8	15.8	24.5	10.7	14.9	12.5
		Low	8.6	8.0	11.7	6.0	7.6	6.2
Summer	Surface	High	4.0	4.0	7.9	0.7	4.2	4.4
		Low	1.0	1.3	2.3	0.1	1.0	0.9
	Bottom	High	32.8	32.5	39.2	26.6	25.9	15.2
		Low	5.3	5.3	7.0	3.8	3.9	2.1
Fall	Surface	High	2.1	2.8	6.0	0.1	2.1	2.1
		Low	0.1	0.3	1.3	0	0.1	0.1
	Bottom	High	2.5	2.5	3.8	1.2	2.1	1.4
		Low	0.5	0.5	0.6	0.4	0.4	0.3

Table S4. Percentage of suboptimal Ω_{Ar} values [Ω_{Ar}<2] over the inner-shelf between 93º–89ºW during high and low discharge conditions as derived from the model hindcast, and the five sensitivity experiments: Constant Carbonate (CCBN), Alkalinity 90% (Alk090), Alkalinity 110% (Alk110), Nitrate 80% (N80), and Nitrate 50% (N50). Estimates are for the period 2000-2019.

.